A&A 600, A128 (2017)
DOI: 10.1051/0004-6361/201630260
© ESO 2017

Astronomy & Astrophysics

Surface-effect corrections for oscillation frequencies of evolved stars

W. H. Ball[1,2,3] and L. Gizon[2,1,4]

[1] Institut für Astrophysik, Georg-August-Universität Göttingen, Friedrich-Hund-Platz 1, 37077 Göttingen, Germany
[2] Max-Planck-Institut für Sonnensystemforschung, Justus-von-Liebig-Weg 3, 37077 Göttingen, Germany
[3] School of Physics and Astronomy, University of Birmingham, Edgbaston, Birmingham, B15 2TT, UK
e-mail: wball@bison.ph.bham.ac.uk
[4] Center for Space Science, NYUAD Institute, New York University Abu Dhabi, PO Box 129188, Abu Dhabi, UAE

Received 15 December 2016 / Accepted 5 February 2017

ABSTRACT

Context. Accurate modelling of solar-like oscillators requires that modelled mode frequencies are corrected for the systematic shift caused by improper modelling of the near-surface layers, known as the surface effect. Several parametrizations of the surface effect are now available but they have not yet been systematically compared with observations of stars showing modes with mixed g- and p-mode character.

Aims. We investigate how much additional uncertainty is introduced to stellar model parameters by our uncertainty about the functional form of the surface effect. At the same time, we test whether any of the parametrizations is significantly better or worse at modelling observed subgiants and low-luminosity red giants.

Methods. We model six stars observed by *Kepler* that show clear mixed modes. We fix the input physics of the stellar models and vary the choice of surface correction between five parametrizations.

Results. Models using a solar-calibrated power law correction consistently fit the observations more poorly than the other four corrections. Models with the remaining four corrections generally fit the observations about equally well, with the combined surface correction by Ball & Gizon perhaps being marginally superior. The fits broadly agree on the model parameters within about the 2σ uncertainties, with discrepancies between the modified Lorentzian and free power law corrections occasionally exceeding the 3σ level. Relative to the best-fitting values, the total uncertainties on the masses, radii and ages of the stars are all less than 2, 1 and 6 per cent, respectively.

Conclusions. A solar-calibrated power law, as formulated by Kjeldsen et al., appears unsuitable for use with more evolved solar-like oscillators. Among the remaining surface corrections, the uncertainty in the model parameters introduced by the surface effects is about twice as large as the uncertainty in the individual fits for these six stars. Though the fits are thus somewhat less certain because of our uncertainty of how to manage the surface effect, these results also demonstrate that it is feasible to model the individual mode frequencies of subgiants and low-luminosity red giants, and hence also use these individual stars to help to constrain stellar models.

Key words. asteroseismology – stars: oscillations

1. Introduction

Space-based observations by CoRoT (Auvergne et al. 2009) and *Kepler* (Borucki et al. 2010) have led to the measurement and analysis of oscillation mode frequencies in dozens of dwarf solar-like oscillators (e.g. Lund et al. 2017; Silva Aguirre et al. 2017). However, to fully exploit these observations, one must correct for a systematic difference between modelled and observed mode frequencies caused by improper modelling of the near-surface layers of these stars. This difference is known as the "surface effect" or "surface term" and, if not corrected, ultimately biases the stellar properties that are inferred.

Broadly speaking, the surface effect can be mitigated either by applying some sort of correction to the computed frequencies or by trying to model the stars and their oscillations better in the first place. Along the first line, Kjeldsen et al. (2008) proposed to correct the model frequencies using a solar-calibrated power law, which has subsequently been used quite widely (e.g. Metcalfe et al. 2012; Deheuvels et al. 2014). More recently, Ball & Gizon (2014) proposed a correction of the form $\nu^3/\mathcal{I}$, possibly supplemented by a term of the form $\nu^{-1}/\mathcal{I}$, where ν is the (cyclic) mode frequency and $\mathcal{I}$ the mode inertia normalized at the photosphere. Finally, Sonoi et al. (2015) proposed a modified Lorentzian correction.

There has not been a systematic comparison of all of these parametrized corrections in main-sequence stars. Ball & Gizon (2014) compared their proposed corrections with the solar-calibrated power law of Kjeldsen et al. (2008) and found that their one-term correction reproduced the solar surface effect better and also provided better-fitting models for the G0V CoRoT target HD 52265. The additional term did not improve the fit significantly. They showed that the solar-calibrated power-law correction tends to overpredict the magnitude of the surface correction at frequencies below about 2500 μHz or above 3500 μHz and a similar trend was the main reason for the poor fits to HD 52265.

Schmitt & Basu (2015) compared the surface corrections of Kjeldsen et al. (2008) and Ball & Gizon (2014), as well as a scaled solar surface term (with or without an additive constant), by fitting frequency differences between different published solar models, between solar models calibrated with different model atmospheres, and between stellar models in a large

grid before and after modifying their near-surface structure. The two-term correction by Ball & Gizon (2014) was best at fitting the differences between the published solar models and only marginally worse than a scaled solar surface term, with an additive constant, at fitting the differences between solar models calibrated with different atmospheres. For the grid of stellar models, Schmitt & Basu (2015) found that, depending on how they modified the near-surface layers, either all the surface corrections performed similarly well or the two-term correction by Ball & Gizon (2014) was clearly superior. The modified Lorentzian of Sonoi et al. (2015) was not yet published and thus not considered in their comparison.

Along a similar line to parametrizing the surface correction, Roxburgh & Vorontsov (2003) proposed to mitigate the surface effect by instead considering ratios of frequency differences, specifically constructed to cancel out the individual modes' sensitivities to the near-surface layers. Otí Floranes et al. (2005) demonstrated that these "separation ratios" are mostly sensitive to a star's core and they have also seen frequent use (e.g. Reese et al. 2016; Silva Aguirre et al. 2017). Roxburgh (2015, 2016) has suggested new methods based on the same underlying principles but these are too new to have seen use.

The last few years have seen a renewed effort towards the second approach: improving the models of the near-surface layers, usually by supplementing the stellar models with averaged structures from three-dimensional radiation hydrodynamics (3D RHD) simulations. The process of replacing the near-surface layers of an existing model with averaged 3D RHD simulation data is now usually referred to as "patching" and authors now present differences between "patched" and "unpatched" models.

Rosenthal et al. (1999) computed frequency differences between mixing-length models of the Sun's convective envelope before and after patching. They found the mode frequencies matched the observations better (if one assumes that the perturbation to the turbulent pressure behaves in the same way as the perturbation to the gas pressure) but a significant – though smaller – systematic difference remained. Piau et al. (2014) presented the first frequency differences for patched models of the whole Sun, corroborating the original conclusions of Rosenthal et al. (1999). Most recently, Magic & Weiss (2016) compared the frequencies with different magnetic field strengths included in the 3D RHD simulations. Finally, Sonoi et al. (2015) and Ball et al. (2016), using different 3D RHD and stellar model codes, computed frequency differences using patched models for stellar types other than the Sun, broadly finding larger surface effects for hotter stars. Sonoi et al. (2015) also found smaller surface effects for less compact stars (i.e. stars with lower surface gravities).

These calculations, however, are all limited to the structural part of the surface effect. It is also expected that some of the surface effect is caused by the interaction between convection and pulsation. Houdek et al. (2017) considered these effects for a model of the solar envelope, using a non-local theory of convection, and found that, once full account is taken of various non-adiabatic and dynamical effects, the difference between the modelled and observed frequencies improves further still. A residual difference persists but these calculations can still be refined and bode well.

Most of the discussion of surface effects so far has considered the Sun and dwarf stars without any mixed modes. These are modes that have oscillating components both in the outer layers of the star as well as in the stellar core, separated by an evanescent region. The outer oscillating components correspond to p-modes, as observed in dwarf stars like the Sun, whereas the inner oscillating components correspond to g-modes. In unevolved stars, like the Sun, the p-mode and g-mode oscillations are confined to distinct ranges of frequencies but, as a star evolves, the p-mode frequencies decrease while the g-mode frequencies increase, and it becomes possible for the modes to couple into a mixed mode with minimal damping between. Such a mode then has an observable amplitude at the surface and its mixed nature is revealed by the mode frequency's deviation from the usual pattern for p-modes.

Evolved red giants show dense spectra of mixed modes that are being exploited to infer a tremendous amount of information about the stars' cores (see e.g. Hekker & Christensen-Dalsgaard 2016, for a recent review) but smaller numbers of mixed modes are also detected in subgiants and low-luminosity red giants. These modes are potentially problematic for pipelines that are now standard for modelling dwarf solar-like oscillators, to the extent that stars in these samples that show too many mixed modes are omitted (e.g. Metcalfe et al. 2014; Lund et al. 2017). Modelling individual mixed modes in more evolved stars is even more challenging. Recent efforts typically use derived parameters (e.g. the asymptotic period spacing) instead of the individual mixed mode frequencies (e.g. Pérez Hernández et al. 2016).

Our current interest is the nature of the surface effect in these stars and their mixed modes. The mixed modes' frequencies are determined in part by the stellar core, which is presumably oblivious to the star's near-surface structure. We therefore expect that these modes will show smaller frequency shifts as a result of the surface effects but this has not yet been tested, and it is not obvious that the parametrizations that have worked for dwarfs will continue to work in more evolved stars.

Here, we consider surface corrections in six subgiant stars, originally studied by Deheuvels et al. (2014) precisely for their mixed modes: KIC 12508433, KIC 8702606, KIC 5689820, KIC 8751420, KIC 7799349 and KIC 9574283. We compare best-fitting stellar models with five different surface corrections with the aim of determining how much uncertainty is induced on the stellar parameters by our uncertainty about the surface effect, and to see if one correction might be obviously better (or worse) than the others. We do not consider the correction methods proposed by Roxburgh & Vorontsov (2003) and Roxburgh (2015, 2016) because the underlying assumption of the oscillations being in one cavity is not satisfied.

2. Methods

2.1. Stellar models

We computed stellar models using the Modules for Experiments in Stellar Astrophysics (MESA[1], revision 7624; Paxton et al. 2011, 2013, 2015). Opacities are taken at high- and low-temperatures from the tables of the OPAL collaboration (Iglesias & Rogers 1996) and Ferguson et al. (2005), respectively. The equation of state is MESA's default, the relevant part of which is principally based on the OPAL EOS (Rogers & Nayfonov 2002). Nuclear reaction rates are taken from the NACRE tables (Angulo et al. 1999) or, if not available there, from the tables by Caughlan & Fowler (1988). For the specific reactions $^{14}\mathrm{N}(p,\gamma)^{15}\mathrm{O}$ and $^{12}\mathrm{C}(\alpha,\gamma)^{16}\mathrm{O}$, we use revised rate by Imbriani et al. (2005) and Kunz et al. (2002) (though the latter is not relevant here). Convection is described by mixing-length theory (Böhm-Vitense 1958) as presented in Cox & Giuli (1968). Gravitational settling is implemented according to Thoul et al. (1994); radiative levitation is neglected.

[1] http://mesa.sourceforge.net

The solar metal mixture is that of Grevesse & Sauval (1998). Finally, the surface boundary condition is determined by integrating a standard Eddington-grey atmosphere from an optical depth of $\tau = 10^{-4}$ to the photospheric value of $\tau = 2/3$ and the atmospheric structure is included in the stellar model when computing the mode frequencies. We computed linear adiabatic mode frequencies using the Aarhus adiabatic pulsation code (ADIPLS, Christensen-Dalsgaard 2008). All models were remeshed to contain 4800 meshpoints before the frequencies were computed (from typically about 2000 meshpoints during the evolution). The remeshing used the remeshing routine bundled with ADIPLS (Christensen-Dalsgaard & Berthomieu 1991), which uses the asymptotic behaviour of the modes to redistribute points more evenly over the displacement eigenfunction. Without remeshing, oscillation codes are known to sometimes miss mixed modes.

2.2. Surface terms

We modelled the stars using five different surface corrections, which each provide corrected model frequencies $\nu_{\rm cor}$ in terms of the uncorrected model frequencies $\nu_{\rm mdl}$ such that they should better match the observed frequencies $\nu_{\rm obs}$.

First, we used the solar-calibrated power law of Kjeldsen et al. (2008), with the power-law index fixed at a value of $p_1 = 5.00$ using a solar calibration with the same input physics as above. This is a typical value for the parameter: Kjeldsen et al. (2008) themselves found $p_1 = 4.90$. The correction is then

$$r\nu_{\rm cor} - \nu_{\rm mdl} = \frac{p_0}{Q}\left(\frac{\nu_{\rm mdl}}{\nu_{\rm ref}}\right)^{p_1} \tag{1}$$

where r is the ratio of the square roots of the modelled and observed mean densities and $\nu_{\rm ref}$ is a reference frequency, taken here to be $\nu_{\rm max}$, the frequency of maximum oscillation power, determined from the scaling relation (Kjeldsen & Bedding 1995)

$$\nu_{\rm max} = \frac{g}{g_\odot}\left(\frac{T_{\rm eff}}{T_{\rm eff,\odot}}\right)^{-1/2}\nu_{\rm max,\odot} \tag{2}$$

with $\log g_\odot = 4.438$, $T_{\rm eff,\odot} = 5777$ K and $\nu_{\rm max,\odot} = 3090\ \mu$Hz. The coefficient p_0 is determined in essence by linear regression (see Kjeldsen et al. 2008, for details). In Eq. (1), Q is the ratio between the mode inertia of the mode divided by the inertia that a radial mode would have at the same frequency, determined by linear interpolation. This factor has long been used to capture the variation of the surface effects with mode inertia (Christensen-Dalsgaard 1986).

Second, we used the corrections proposed by Ball & Gizon (2014): their "cubic" correction

$$\nu_{\rm cor} - \nu_{\rm mdl} = a_3\left(\frac{\nu_{\rm mdl}}{\nu_{\rm ac}}\right)^3/\mathcal{I} \tag{3}$$

and their "combined" correction

$$\nu_{\rm cor} - \nu_{\rm mdl} = \left[a_{-1}\left(\frac{\nu_{\rm mdl}}{\nu_{\rm ac}}\right)^{-1} + a_3\left(\frac{\nu_{\rm mdl}}{\nu_{\rm ac}}\right)^3\right]/\mathcal{I}. \tag{4}$$

Here, $\mathcal{I}$ is the mode inertia normalized at the photosphere, $\nu_{\rm ac}$ is the acoustic cut-off frequency, scaled from a solar value of 5000 μHz (Jiménez et al. 2011) using the scaling relations, and the parameters a_{-1} and a_3 are determined by linear regression to minimize the differences between all the observed and modelled mode frequencies. The acoustic cut-off is used purely to rescale the coefficients a_{-1} and a_3. The correction is based on the asymptotic behaviour of the eigenfunctions near the surface. From the variational principle for linear adiabatic oscillations, Gough (1990) showed that a simple sound speed perturbation would cause a frequency shift of the form $\nu^3/\mathcal{I}$, whereas a perturbation to the pressure scale height would cause a shift of the form $\nu^{-1}/\mathcal{I}$. Ball & Gizon (2014) showed that functions of this form give a better fit to the known solar surface effect than a power law.

Third, we considered a modified Lorentzian correction

$$\nu_{\rm cor} - \nu_{\rm mdl} = \frac{s_0\nu_{\rm max}}{Q}\left[1 - \frac{1}{1 + (\nu_{\rm mdl}/\nu_{\rm max})^{s_1}}\right] \tag{5}$$

as suggested by Sonoi et al. (2015). Rather than use their calibrations of s_0 and s_1 to frequency changes between their patched and unpatched models, we treated them as free parameters, optimized for each stellar model by the Newton–Rhapson method to fit the observed frequencies using all of the observed modes. Sonoi et al. (2015) only considered radial modes in formulating Eq. (5) so we have chosen to include the factor Q, as in the correction by Kjeldsen et al. (2008). Also, after performing a large number of fits, we found that the best-fitting models for stars B and D had positive values of s_0 and negative values of s_1, which corresponds to a surface correction of opposite sign to the Sun and decreasing in magnitude with increasing frequency. We regard this as unphysical and subsequently restricted the fits to have $s_1 > 0$.

Finally, we also included a free power law, as in Eq. (1) but with both p_0 and p_1 as free parameters and with r fixed to 1. The quality of these fits gives us some idea of how much we are gaining from more complicated models of the surface term. As with the modified Lorentzian, solutions with $p_1 < 0$ correspond to surface corrections that decrease in magnitude with increasing frequency, so we restricted our best-fit models to those with $p_1 > 0$.

2.3. Sample of stars

We modelled the six stars studied by Deheuvels et al. (2014), who selected these subgiants and low-luminosity red giants to invert for their rotational profiles. They are KIC 12508433, KIC 8702606, KIC 5689820, KIC 8751420, KIC 7799349 and KIC 9574283, labelled hereafter by letters A through F, in decreasing order of the surface gravity inferred from the global seismic parameters (as in Deheuvels et al. 2014). Basic data is given in Table 1 and their positions in the Hertzsprung–Russell diagram are shown in Fig. 1, where the luminosities have been inferred from scaling relations.

Rotational inversions require several features of the observations. The stars have high signal-to-noise ratios and clear mixed modes, for which the rotational splitting is well-resolved. The stars could feasibly be modelled to identify which frequency corresponds to which mode. As stars ascend the red giant branch, they develop an ever denser spectrum of mixed modes and matching the correct modelled mode to the observed mode frequency becomes ambiguous, which ruled out more evolved stars. Our study also requires stars with clear mixed modes and high signal-to-noise ratio in all the observed modes, so it is clear that these six stars are suitable.

At first, we used all of the frequencies and their uncertainties given by Deheuvels et al. (2014). We found that we could

Table 1. Global seismic and non-seismic parameters for the six subgiants studied in this article.

Star	KIC	$T_{\rm eff}$/K	[Fe/H]	$\Delta\nu/\mu$Hz	$\nu_{\rm max}/\mu$Hz
A	KIC 12508433	5248 ± 130	0.25 ± 0.23	45.3 ± 0.2	793 ± 21
B	KIC 8702606	5540 ± 60	-0.09 ± 0.06	39.9 ± 0.4	664 ± 14
C	KIC 5689820	4978 ± 167	0.24 ± 0.16	41.0 ± 0.3	695 ± 15
D	KIC 8751420	5264 ± 60	-0.15 ± 0.06	34.7 ± 0.4	598 ± 14
E	KIC 7799349	5115 ± 60	0.41 ± 0.06	33.7 ± 0.4	561 ± 8
F	KIC 9574283	5120 ± 55	-0.40 ± 0.08	30.0 ± 0.5	455 ± 8

Notes. The effective temperatures and metallicities are taken from the spectroscopic values in Table 10 of Deheuvels et al. (2014). The large separations $\Delta\nu$ and frequencies of maximum oscillation power $\nu_{\rm max}$ are from their Table 1.

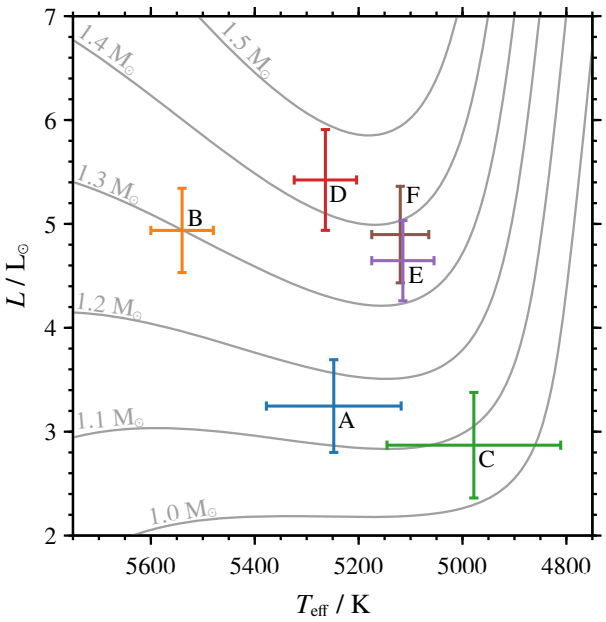

Fig. 1. Locations of the six stars under study in the Hertzsprung–Russell diagram using luminosities that have been computed using scaling relations. The solid lines are evolutionary tracks for stellar models using a solar-calibrated mixing-length parameter and composition for mass from 1.0 to 1.5 $M_\odot$ in steps of 0.1 $M_\odot$. The sample of stars are all located towards the end of the subgiant branch or at the base of the red giant branch.

Table 2. Mode frequencies that were excluded in the analysis because of poor initial fits.

Star	Frequency/μHz	ℓ
B	491.070 ± 0.024	0
C	511.857 ± 0.011	2
E	511.478 ± 0.032	2
F	398.982 ± 0.021	1

not reasonably model stars B, C, E and F as long as we included the worst-fitting modes, which contributed more than half of the total χ^2 for each star, and sometimes nearly all of it. We therefore removed these modes from our data. The frequencies and angular degrees of the excluded modes are given in Table 2. Of course, rejecting the data that fits worst will inevitably give better fits. However, in these cases we specifically found that the poorly fitting modes dominated χ^2 so much that they were clearly biasing the results away from models that were much better able to reproduce the other mode frequencies. We kept other mode frequencies that appear consistently discrepant, since those modes did not appear to bias our results away from models that could fit the remaining data. e.g. the highest-frequency mode in star F (ν = 581.219 μHz).

2.4. Fitting method

We fit the stellar models using essentially the same method presented in other studies to which we contributed best fit models (e.g. Appourchaux et al. 2015; Reese et al. 2016). We optimized the total χ^2 of the observations, defined by

$$\chi^2 = \sum_{i=1}^{N_{\rm obs}} \left(\frac{y_{{\rm obs},i} - y_{{\rm mdl},i}}{\sigma_i} \right)^2 \tag{6}$$

where $y_{{\rm obs},i}$, $y_{{\rm mdl},i}$ and σ_i are the observed value, modelled value and observed uncertainty of the ith observable. Here, these are the effective temperature $T_{\rm eff}$, the metallicity $[{\rm Fe/H}]_{\rm s}$ (see Table 1) and the individual mode frequencies. Specifically, we did not weight any part of χ^2 by any additional factor.

We first estimated some stellar parameters using coarse grid-based modelling before moving onto an iterative method. For each set of mass M, initial helium abundance Y_0, initial metallicity $[{\rm Fe/H}]_0$ and mixing-length parameter α, we started an evolutionary track from a chemically-homogeneous pre-main-sequence model with central temperature 9×10^5 K. The timestep was gradually reduced as the stellar model first matched the spectroscopic parameters and then the radial mode frequencies. At this point, all the mode frequencies were computed and the total χ^2 evaluated. The main difference between the current and previous optimizations (all for main-sequence or near-main-sequence stars) was that the minimum timestep was reduced to as little as 3200 yr in order to compute models during the rapid evolution of the mixed mode frequencies.

Next, we performed iterations of the Nelder–Mead downhill simplex method (Nelder & Mead 1965), with additional linear extrapolations to explore parameter space, and recorded each set of model parameters that were tried. When the next step of the downhill simplex would have been a contraction step, we tried to generate better-fitting model parameters by various methods, including: linear extrapolations from random subsamples of the sample so far; small, dense grids spanning the present estimate of the 1σ to 5σ confidence regions; or random uniform samples within the 1σ to 5σ confidence regions. When nothing seemed to improve the fit any further, the best-fitting model parameters were used for an uninterrupted standard downhill simplex to check that we had found at least a locally-optimal model.

The above process, though somewhat haphazard, was aimed at preventing convergence on a local minimum, which we sometimes find is a problem. Though we cannot guarantee that our best-fitting models are not local minima, our extensive searches

Table 3. Model parameters with uncertainties for fits for each of the six stars and five surface corrections.

Name	Corr.	t/Gyr	$M/M_\odot$	Y_0	$[\mathrm{Fe/H}]_0$	α	Surface correction parameters	
	c	5.15 ± 0.13	1.290 ± 0.012	0.256 ± 0.007	0.093 ± 0.033	2.07 ± 0.05	−4.70 ± 0.13	
	b	5.07 ± 0.13	1.293 ± 0.010	0.255 ± 0.005	0.081 ± 0.029	2.09 ± 0.05	2.00 ± 0.61	−4.75 ± 0.07
A	s	5.59 ± 0.14	1.262 ± 0.009	0.271 ± 0.005	0.191 ± 0.027	1.92 ± 0.04	−4.18 ± 0.18	10.70 ± 0.68
	p	4.82 ± 0.09	1.310 ± 0.006	0.244 ± 0.003	0.015 ± 0.021	2.20 ± 0.04	−2.08 ± 0.15	3.96 ± 0.22
	k	4.98 ± 0.03	1.438 ± 0.005	0.178 ± 0.003	−0.067 ± 0.007	2.22 ± 0.01	−0.00 ± 0.02	
	c	3.86 ± 0.02	1.260 ± 0.010	0.266 ± 0.006	−0.184 ± 0.016	2.06 ± 0.03	−6.98 ± 0.21	
	b	3.84 ± 0.03	1.248 ± 0.009	0.270 ± 0.004	−0.199 ± 0.017	2.10 ± 0.03	−3.95 ± 0.73	−7.14 ± 0.21
B	s	3.89 ± 0.03	1.266 ± 0.015	0.263 ± 0.008	−0.179 ± 0.020	2.04 ± 0.03	−6.49 ± 0.53	9.58 ± 0.82
	p	3.74 ± 0.02	1.240 ± 0.006	0.270 ± 0.003	−0.248 ± 0.015	2.23 ± 0.03	−3.47 ± 0.61	2.64 ± 0.50
	k	3.61 ± 0.02	1.389 ± 0.006	0.216 ± 0.003	−0.246 ± 0.006	2.22 ± 0.01	−0.41 ± 0.04	
	c	7.36 ± 0.07	1.152 ± 0.007	0.268 ± 0.003	0.104 ± 0.008	1.99 ± 0.01	−6.84 ± 0.12	
	b	7.35 ± 0.10	1.152 ± 0.008	0.268 ± 0.004	0.103 ± 0.009	1.99 ± 0.01	−0.27 ± 0.62	−6.80 ± 0.11
C	s	7.40 ± 0.07	1.178 ± 0.007	0.255 ± 0.003	0.098 ± 0.009	1.97 ± 0.01	−5.91 ± 0.32	9.05 ± 0.41
	p	6.79 ± 0.10	1.116 ± 0.010	0.285 ± 0.004	0.046 ± 0.014	2.12 ± 0.02	−4.43 ± 0.36	2.47 ± 0.16
	k	7.39 ± 0.05	1.101 ± 0.005	0.295 ± 0.003	0.145 ± 0.006	1.99 ± 0.01	−1.71 ± 0.02	
	c	4.25 ± 0.05	1.286 ± 0.010	0.226 ± 0.006	−0.319 ± 0.019	2.07 ± 0.02	−8.62 ± 0.18	
	b	4.28 ± 0.05	1.292 ± 0.010	0.223 ± 0.006	−0.310 ± 0.017	2.04 ± 0.02	3.22 ± 0.93	−8.47 ± 0.20
D	s	4.20 ± 0.07	1.315 ± 0.008	0.211 ± 0.005	−0.357 ± 0.014	2.10 ± 0.02	−5.68 ± 0.44	8.62 ± 0.65
	p	4.39 ± 0.07	1.286 ± 0.009	0.217 ± 0.005	−0.352 ± 0.012	2.09 ± 0.02	−2.35 ± 0.18	3.26 ± 0.16
	k	4.03 ± 0.05	1.365 ± 0.004	0.195 ± 0.002	−0.371 ± 0.007	2.11 ± 0.01	−0.76 ± 0.01	
	c	3.75 ± 0.17	1.495 ± 0.010	0.233 ± 0.005	0.132 ± 0.014	1.94 ± 0.04	−7.08 ± 0.20	
	b	4.09 ± 0.26	1.463 ± 0.008	0.239 ± 0.008	0.176 ± 0.014	1.89 ± 0.06	−2.92 ± 0.92	−7.26 ± 0.31
E	s	4.05 ± 0.13	1.463 ± 0.009	0.240 ± 0.004	0.177 ± 0.011	1.89 ± 0.03	−7.31 ± 0.28	7.28 ± 0.39
	p	4.12 ± 0.18	1.425 ± 0.014	0.248 ± 0.009	0.158 ± 0.008	1.94 ± 0.04	−2.79 ± 0.73	2.77 ± 0.66
	k	3.99 ± 0.04	1.639 ± 0.004	0.183 ± 0.001	0.182 ± 0.005	1.73 ± 0.01	0.03 ± 0.06	
	c	7.63 ± 0.20	1.040 ± 0.012	0.245 ± 0.009	−0.408 ± 0.021	1.88 ± 0.02	−13.44 ± 0.73	
	b	7.65 ± 0.20	1.033 ± 0.012	0.249 ± 0.007	−0.397 ± 0.018	1.88 ± 0.02	1.90 ± 1.16	−13.47 ± 0.41
F	s	7.55 ± 0.27	1.063 ± 0.015	0.233 ± 0.005	−0.423 ± 0.015	1.87 ± 0.02	−6.69 ± 0.48	9.41 ± 0.56
	p	7.07 ± 0.16	1.057 ± 0.013	0.240 ± 0.006	−0.472 ± 0.012	1.96 ± 0.02	−2.08 ± 0.16	3.43 ± 0.21
	k	3.93 ± 0.07	1.261 ± 0.003	0.231 ± 0.002	−0.478 ± 0.005	2.35 ± 0.01	0.02 ± 0.01	

Notes. The surface corrections "c", "b", "s", "p" and "k" refer to the cubic and combined terms of Ball & Gizon (2014), the modified Lorentzian of Sonoi et al. (2015), a free power law and the solar-calibrated power law by Kjeldsen et al. (2008). The surface correction parameters in each of the five cases are $a_3/10^{-7}$ μHz (Eq. (3)), $a_{-1}/10^{-8}$ μHz and $a_3/10^{-7}$ μHz (Eq. (4)), $s_0/10^{-3}$ μHz and s_1 (Eq. (5)), p_0/μHz and p_1 (Eq. (1), $r \equiv 1$), and finally $p_0/r/\mu$Hz (Eq. (1). The model parameters are the age t, mass M, initial helium abundance Y_0, initial metallicity $[\mathrm{Fe/H}]_0$ and mixing-length parameter α.

around the best-fit parameters give us some confidence that they are probably not local minima. We determined uncertainties from ellipsoids bounding surfaces of constant χ^2, finding ellipsoids that would simultaneously enclose all parameters in the sample within the region appropriate to the corresponding value of χ^2. In other words, given a best fit with $\chi^2 = \chi_0^2$, we required that if a sample with $\chi_0^2 + 1$ was contained in the 1σ ellipsoid, a sample with $\chi_0^2 + 4$ had to simultaneously be contained in the corresponding 2σ ellipsoid. To determine the uncertainties of derived parameters (e.g. radius or effective temperature) we performed a linear fit of the derived parameters relative to the model parameters and used linear propagation of uncertainties.

3. Results for individual stars

3.1. Results and discussion

Our results are given in Tables 3 and 4 for each star from A to F and each surface correction, labelled by "c", "b", "s", "p", "k" for the cubic correction, combined correction, modified Lorentzian, free power law and solar-calibrated power law, respectively. Table 3 lists the stellar model parameters, including the relevant free parameters for each of the surface corrections. Table 4 lists the derived parameters, which can be compared to the row of observational values labelled by "o". The effective temperature T_{eff} and surface metallicity $[\mathrm{Fe/H}]_{\mathrm{s}}$ are given by Deheuvels et al. (2014); the other parameters are derived from scaling relations. Table 4 also gives the total misfit χ^2 (i.e. Eq. (6)) and reduced misfit $\chi_r^2 = \chi^2/N_{\mathrm{d.o.f.}}$, where $N_{\mathrm{d.o.f.}}$ is the number of observations less the number of free parameters. Figures 2 to 6 show the frequency differences between the best fitting models for each star and each surface effect, both before and after the correction is applied. Each figure shows the fits for one surface correction, in the same order as in Tables 3 and 4.

In all the stars, the inclusion of the mode inertia in the surface correction is clearly important. In Figs 2 to 5, the greatest surface correction is clear for the low-inertia radial and p-dominated mixed modes. The corrections for the less p-dominated mixed

Table 4. Observed quantities and predictions for each of the six stars with the five different surface corrections.

Name	Corr.	$T_{\rm eff}$/K	$\log g$	$[{\rm Fe/H}]_s$	$L/L_\odot$	$R/R_\odot$	χ^2	χ^2_r
	o	5248 ± 130	3.826 ± 0.013	0.250 ± 0.230	3.246 ± 0.445	2.175 ± 0.070		
	c	5409 ± 51	3.835 ± 0.001	0.073 ± 0.032	3.983 ± 0.173	2.275 ± 0.008	229.5	10.9
	b	5434 ± 47	3.834 ± 0.001	0.061 ± 0.028	4.065 ± 0.158	2.277 ± 0.006	204.5	10.2
A	s	5255 ± 45	3.831 ± 0.001	0.170 ± 0.026	3.495 ± 0.141	2.258 ± 0.006	325.6	16.3
	p	5545 ± 37	3.837 ± 0.001	−0.005 ± 0.021	4.443 ± 0.126	2.287 ± 0.004	237.9	11.9
	k	5532 ± 10	3.848 ± 0.000	−0.086 ± 0.007	4.706 ± 0.035	2.364 ± 0.003	4467.4	212.7
	o	5540 ± 60	3.761 ± 0.010	−0.090 ± 0.060	4.935 ± 0.404	2.413 ± 0.075		
	c	5708 ± 21	3.757 ± 0.001	−0.207 ± 0.016	5.764 ± 0.103	2.458 ± 0.006	308.6	14.0
	b	5746 ± 26	3.757 ± 0.001	−0.223 ± 0.017	5.865 ± 0.112	2.447 ± 0.006	258.3	12.3
B	s	5690 ± 28	3.758 ± 0.002	−0.201 ± 0.020	5.713 ± 0.130	2.462 ± 0.010	401.1	19.1
	p	5846 ± 25	3.756 ± 0.001	−0.272 ± 0.015	6.250 ± 0.101	2.440 ± 0.005	297.2	14.2
	k	5811 ± 9	3.769 ± 0.001	−0.268 ± 0.006	6.636 ± 0.044	2.544 ± 0.004	2510.7	114.1
	o	4978 ± 167	3.758 ± 0.013	0.240 ± 0.160	2.870 ± 0.511	2.268 ± 0.074		
	c	5098 ± 12	3.773 ± 0.001	0.084 ± 0.008	3.231 ± 0.029	2.307 ± 0.005	19.7	1.2
	b	5100 ± 14	3.773 ± 0.001	0.084 ± 0.009	3.236 ± 0.040	2.307 ± 0.006	19.2	1.2
C	s	5075 ± 13	3.776 ± 0.001	0.079 ± 0.009	3.223 ± 0.033	2.325 ± 0.005	36.8	2.3
	p	5247 ± 27	3.770 ± 0.001	0.027 ± 0.014	3.535 ± 0.058	2.278 ± 0.008	53.8	3.4
	k	5114 ± 10	3.767 ± 0.001	0.125 ± 0.006	3.174 ± 0.021	2.272 ± 0.004	457.1	26.9
	o	5264 ± 60	3.704 ± 0.011	−0.150 ± 0.060	5.426 ± 0.486	2.802 ± 0.098		
	c	5433 ± 17	3.688 ± 0.001	−0.333 ± 0.019	5.667 ± 0.095	2.690 ± 0.007	224.7	8.6
	b	5407 ± 19	3.688 ± 0.001	−0.324 ± 0.017	5.582 ± 0.104	2.696 ± 0.008	199.5	8.0
D	s	5461 ± 15	3.690 ± 0.001	−0.370 ± 0.014	5.875 ± 0.077	2.711 ± 0.006	443.8	17.8
	p	5445 ± 21	3.688 ± 0.001	−0.366 ± 0.012	5.708 ± 0.094	2.688 ± 0.007	284.9	11.4
	k	5470 ± 13	3.695 ± 0.000	−0.384 ± 0.007	6.080 ± 0.063	2.749 ± 0.003	1718.1	66.1
	o	5115 ± 60	3.670 ± 0.008	0.410 ± 0.060	4.646 ± 0.385	2.747 ± 0.082		
	c	5056 ± 40	3.689 ± 0.001	0.124 ± 0.014	4.927 ± 0.157	2.896 ± 0.007	223.0	8.9
	b	4989 ± 62	3.686 ± 0.001	0.168 ± 0.014	4.595 ± 0.227	2.873 ± 0.005	153.8	6.4
E	s	4995 ± 29	3.686 ± 0.001	0.169 ± 0.011	4.622 ± 0.109	2.874 ± 0.006	160.8	6.7
	p	5038 ± 44	3.683 ± 0.002	0.150 ± 0.008	4.692 ± 0.143	2.846 ± 0.009	339.9	14.2
	k	4845 ± 9	3.700 ± 0.000	0.174 ± 0.005	4.434 ± 0.035	2.993 ± 0.002	6195.3	247.8
	o	5120 ± 55	3.580 ± 0.009	−0.400 ± 0.080	4.898 ± 0.464	2.814 ± 0.111		
	c	5183 ± 21	3.575 ± 0.002	−0.424 ± 0.022	4.920 ± 0.081	2.754 ± 0.011	64.8	3.2
	b	5182 ± 19	3.574 ± 0.001	−0.412 ± 0.018	4.896 ± 0.085	2.749 ± 0.011	54.9	2.9
F	s	5169 ± 19	3.578 ± 0.002	−0.438 ± 0.015	4.943 ± 0.112	2.776 ± 0.014	131.4	6.9
	p	5267 ± 15	3.578 ± 0.002	−0.487 ± 0.012	5.300 ± 0.067	2.768 ± 0.012	188.1	9.9
	k	5561 ± 8	3.600 ± 0.000	−0.488 ± 0.005	7.468 ± 0.049	2.948 ± 0.003	2378.0	118.9

Notes. The labelling is as in Table 3, with an extra row "o" that gives the observed quantities. The effective temperature $T_{\rm eff}$ and surface metallicity $[{\rm Fe/H}]_s$ are as listed by Deheuvels et al. (2014). The other observables – surface gravity $\log g$, luminosity L and radius R – are derived from the scaling relations. The last two columns give the total χ^2 (Eq. (6)) and χ^2 per degree of freedom.

modes fall between zero and the trend followed by the radial and p-dominated mixed modes. These modes have larger inertia and therefore smaller frequency corrections, and this correctly brings the corrected frequencies in line with the low-inertia modes.

The precise ages (especially for stars B and D) may come as a surprise but are easily understood. In short, the frequencies of the mixed modes evolve quickly and are measured precisely. For example, in our best fit for star A, the mixed mode at 836.040 μHz varies with age at about 1.45 μHz/Myr. Given the observed uncertainty of 0.015 μHz, the modelled mode frequency changes by 1σ in a little over 10 000 yr. In other words, along a single evolutionary track, the uncertainty in the age is about 10 000 yr. Most of the reported uncertainty in age is a result of correlations with other parameters.

The best-fit models generally reproduce the spectroscopic properties within about the 2σ limits of the observations. Star E is an exception, almost certainly because of poor modelling (see Sect. 3.2). The models of stars B and D are somewhat hotter and more metal poor than the spectroscopic determinations suggest, with the discrepancy nearing the 3σ level.

3.2. Gravitational settling without competition

Star E appears to have a mass roughly between 1.4 and 1.6 $M_\odot$. In such stars, gravitational settling significantly (and sometimes completely) depletes the stellar surface of its helium and metals, which is obviously inconsistent with observations. Once off the main-sequence, however, the inward-penetrating convection zone partly restores the initial surface mixture, which allows us

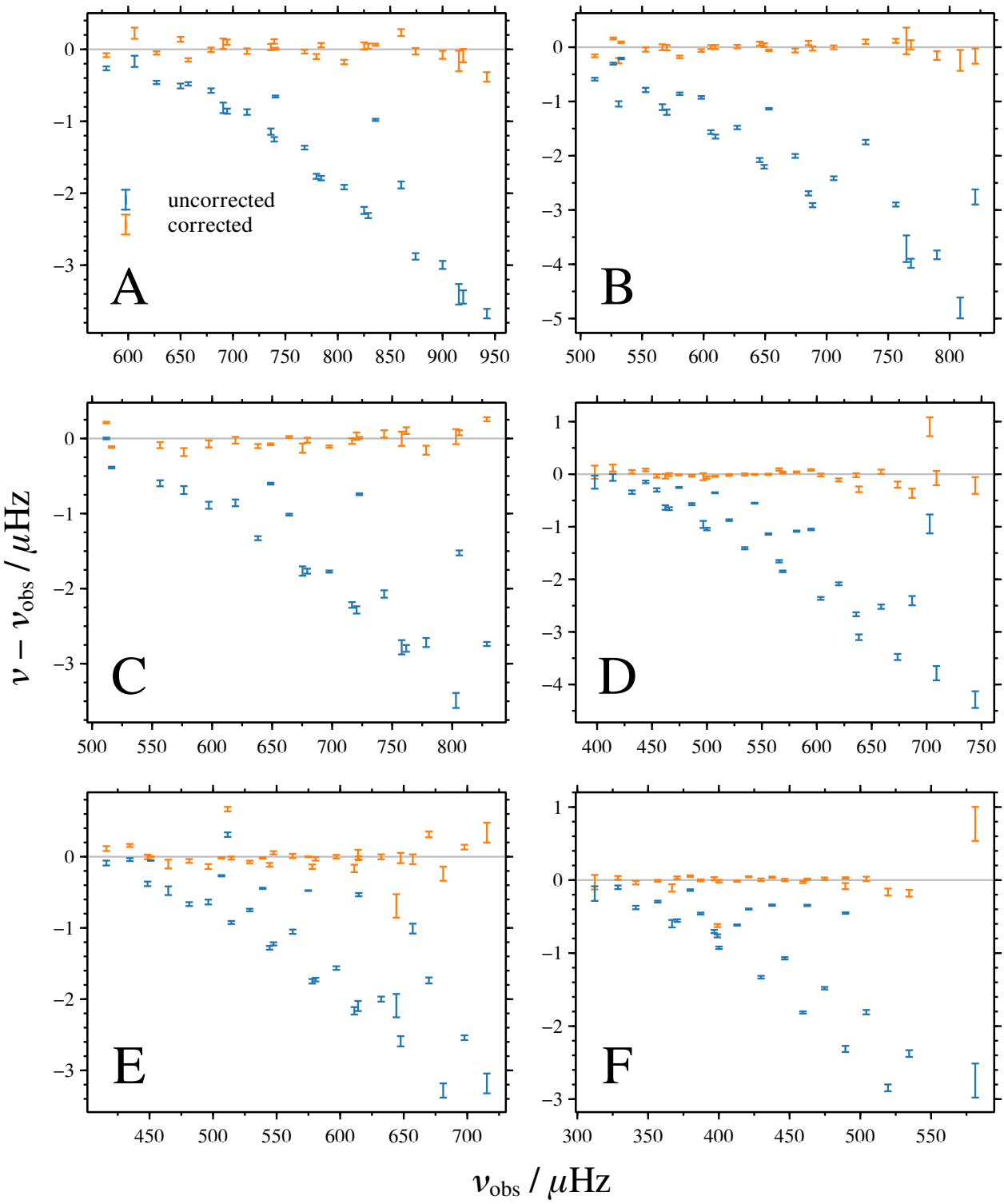

Fig. 2. Differences between modelled and observed frequencies plotted against observed frequency, for best-fitting models using the cubic correction of Ball & Gizon (2014). Each panel corresponds to one of the stars A to F. The blue points are frequency differences before the correction is applied; the orange points after. The error bars are the observed uncertainties in both cases.

to find stellar models that still have reasonable surface metallicities $[\mathrm{Fe/H}]_{\mathrm{s}}$, though usually still inconsistent with the observed value of 0.41 ± 0.06 dex.

In reality, our expectation is that at this mass, some other unmodelled process counteracts the depletion of metals from the stellar atmosphere. Possible competing processes have been studied more extensively in hotter stars – mainly A- and early F-type – and include radiative levitation (e.g. Turcotte et al. 1998), rotation (e.g. Charbonneau & Michaud 1991) or small amounts of mass-loss (e.g. Michaud et al. 2011). Our models of star E, and thus its parameters, exclude these competing processes and should be considered with this in mind. We have included them partly for completeness and partly because we still expect that the characteristics most directly probed by the

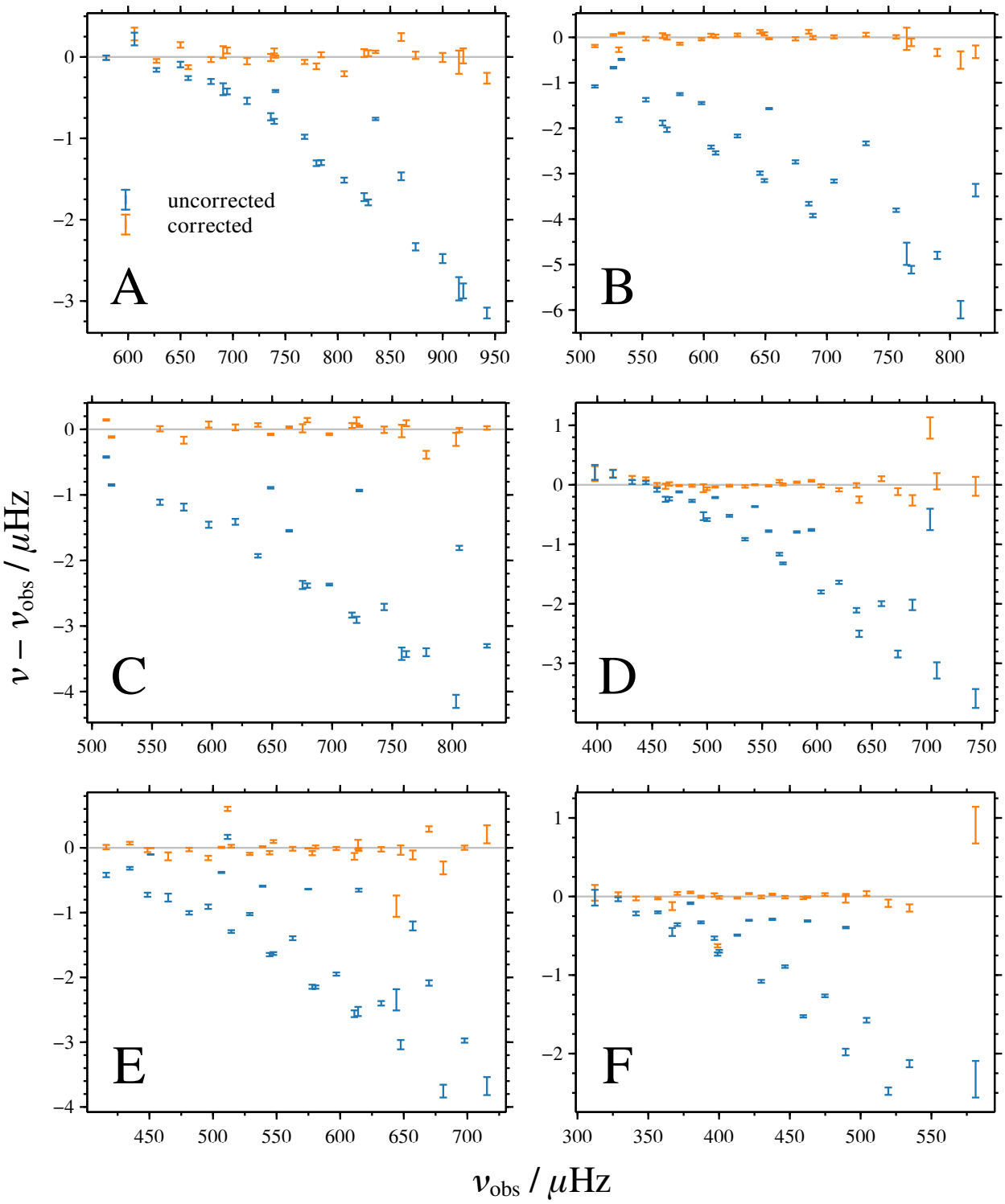

Fig. 3. As in Fig. 2 but for best-fitting models using the combined correction of Ball & Gizon (2014).

mode frequencies (e.g. the mean density and surface gravity) are reasonably accurate, even if the parameters that are interpreted through stellar models (e.g. the age) are not.

Star D is the next most massive star and potentially also suffers from the inclusion of overly-efficient gravitational settling. The initial helium abundance is slightly lower than typical values from Big Bang nucleosynthesis of around 0.247 (e.g. Cyburt et al. 2016) and the observed surface metallicity is discrepant, though not as severely in star E. Star A is also about as massive and the best-fit helium abundance seems low for such a metal-rich star but the surface metallicity is poorly constrained by the spectroscopic observations.

3.3. Which correction is best?

Though no surface effect correction is obviously superior to the others, the solar-calibrated power law by Kjeldsen et al. (2008) fits consistently worse than the other corrections. In fact, in three

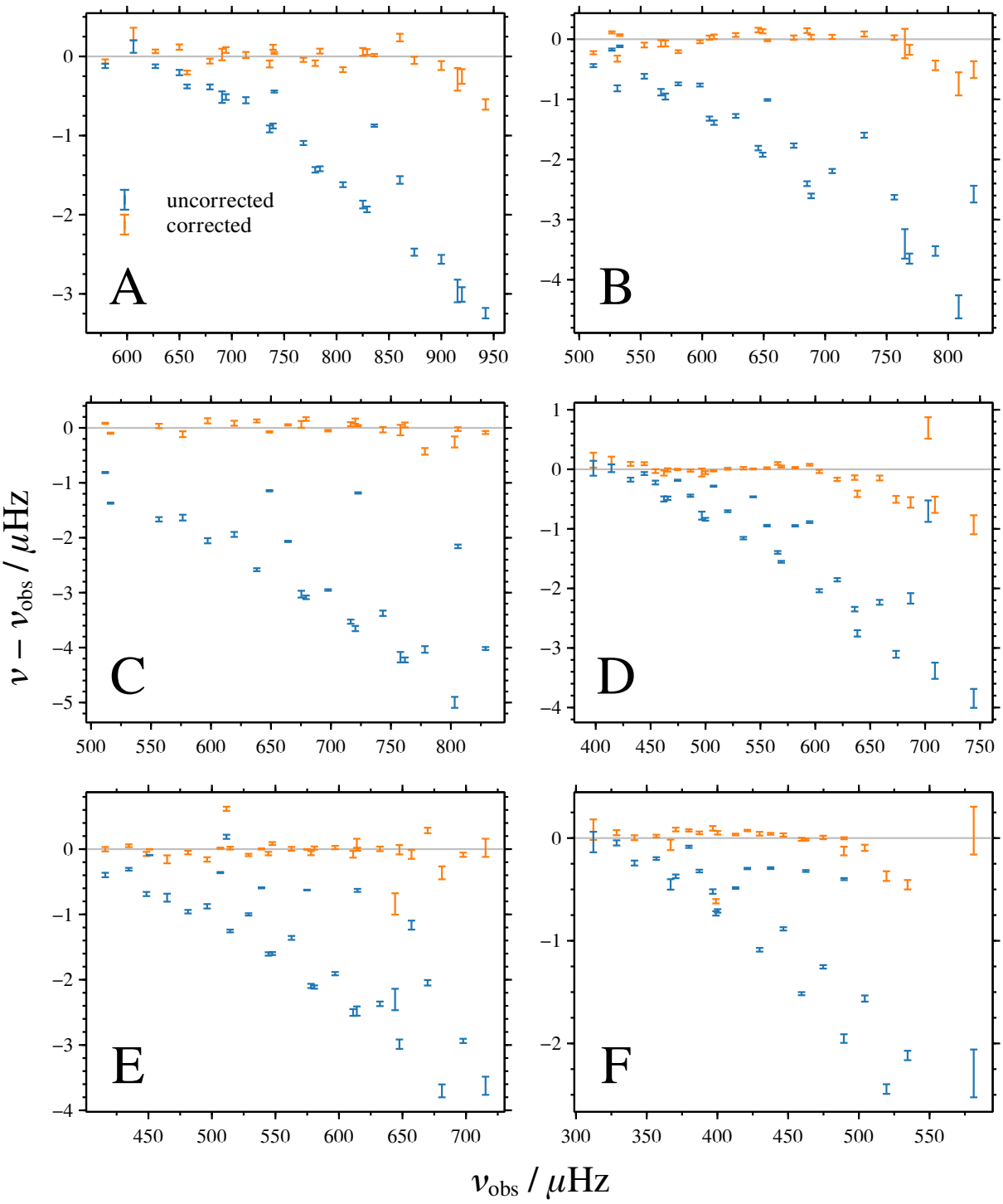

Fig. 4. As in Fig. 2 but for best-fitting models using the modified Lorentzian correction proposed by Sonoi et al. (2015).

cases (stars A, E and F) the best-fitting model is one with no surface correction at all. This result, however, is neither surprising nor an indictment of the calibrated power-law. It is calibrated to the Sun, so while it might be expected to work for Sun-like stars, there is no reason to expect that it would continue to work for these evolved stars. The reasonable results for the uncalibrated power-law show that a simple power law is not a bad idea, it is only using a solar calibration out of context that leads to poor results.

In addition, the formulation of Kjeldsen et al. (2008) first rescales the model frequencies by a factor (originally and here denoted r) that represents the square root of the ratio of the mean densities of the stellar model and the observed star. The best-fitting models using the other corrections imply that the ratio of mean densities is a few thousandths smaller than one. Often, the rescaling is what causes the regression to find that the best-fitting correction is no correction. No other surface correction uses this factor r.

The poor performance of the calibrated power law leads to small uncertainties by our method of estimation, which is based on surfaces of constant χ^2 and therefore assumes that the best-fitting model fits the data reasonably well. When this is not the

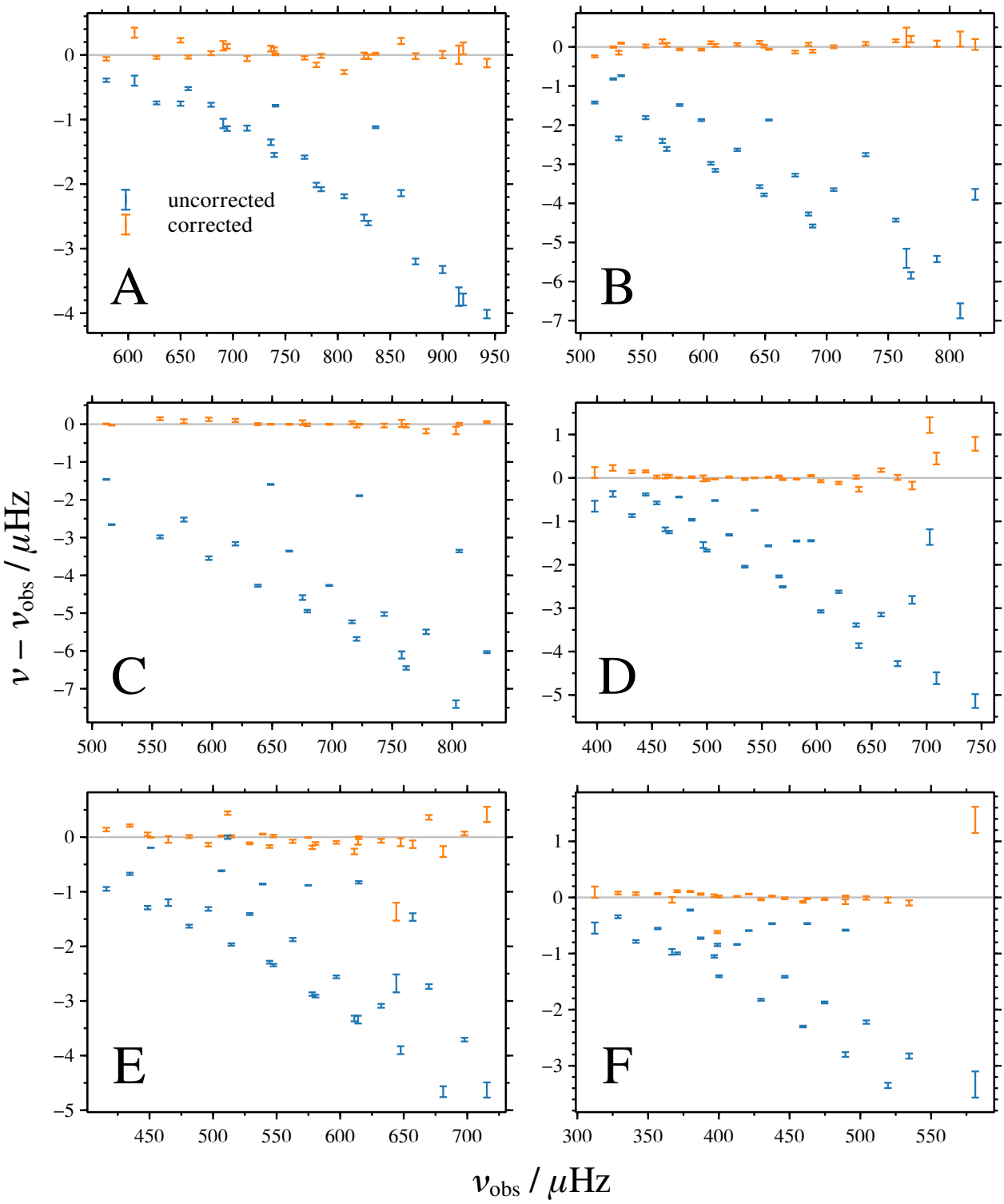

Fig. 5. As in Fig. 2 but for best-fitting models using a free power law.

case, small changes in the model parameters increase χ^2 from a large value to a much larger value and the uncertainty is ultimately underestimated. For this reason, the estimated uncertainties of the surface gravity $\log g$ are sometimes smaller than 0.0005. Since we regard these estimates as unreliable anyway, we have allowed them to be rounded to zero rather than encumber that column of Table 4 with a further significant digit.

Of the other surface corrections, the modified Lorentzian proposed by Sonoi et al. (2015) is the next worst performer in three stars. In many cases, much of the poor performance is contributed by the high-frequency modes, where the modified Lorentzian function fails to capture the continued increase in the scale of the surface effect. For example, in stars A and B, the three highest-frequency modes together contribute 98.3 and 61.7 to χ^2, respectively. Similarly, in star F, the two discrepant modes between 510 and 540 μHz together contribute 71.3 to χ^2. Over the remaining modes, the modified Lorentzian surface term performs about as well as the other corrections. Put differently, the

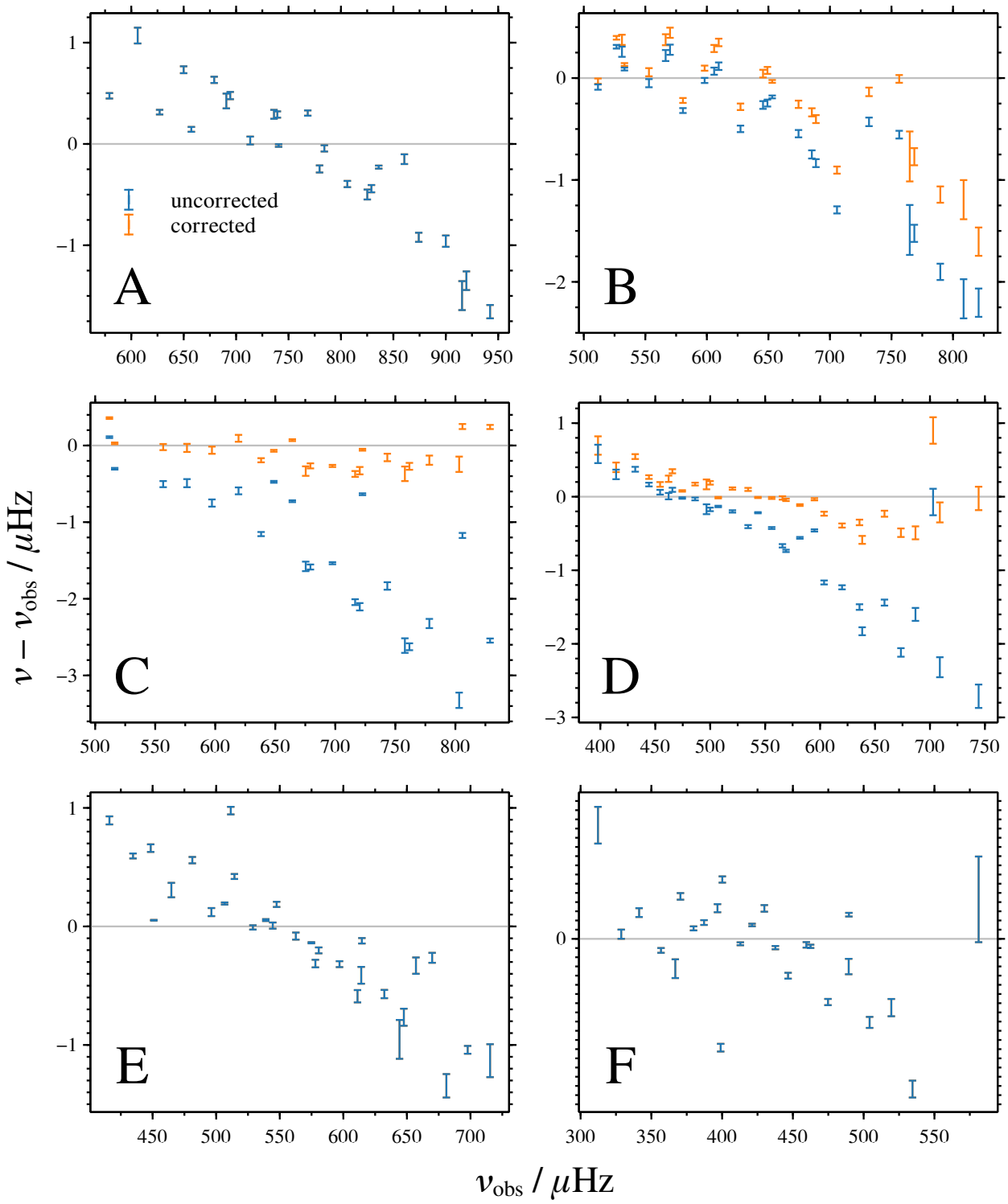

Fig. 6. As in Fig. 2 but for best-fitting models using the solar-calibrated power-law correction of Kjeldsen et al. (2008).

marginally-worse overall performance mostly reflects that the modified Lorentzian does not describe the high-frequency end of the correction very well. The same conclusion can be drawn by comparing the modified Lorentzian with the frequency differences between a solar-calibrated model and low-degree solar mode frequencies.

The free power law is the next best performer but varies between being about as good as the cubic and combined terms (stars A and B) and much worse than the modified Lorentzian (star E). If the index of the power law were fixed at 3, the power law correction would be similar to the cubic term, except for the difference in the treatment of the mode inertia. In the power law, however, the factor Q only corrects for the difference between the inertia of the non-radial modes relative to the radial, whereas the cubic and combined corrections use the mode inertia $\mathcal{I}$ without modification. This difference would be negligible if the mode inertia was roughly a power-law in frequency but it is generally not, except perhaps over small ranges of frequency.

In terms of the χ^2_r, the combined term usually fits best but it is difficult to make robust conclusions when comparing models

that all fit quite badly in absolute terms. Only in star C are the fits sufficiently good that the cubic and combined terms are significantly superior. Our only strong conclusions are that it is inappropriate to use a solar-calibrated power law to correct for surface effects in such evolved stars, and that the modified Lorentzian correction does not match the highest-frequency behaviour of observed surface effects.

3.4. Uncertainty from choice of correction

We investigated the level of uncertainty induced by the choice of surface correction for each star, neglecting the consistently-discrepant solar-calibrated power law, first by combining the uncertainties derived for each surface correction in quadrature and comparing the spread of 1σ confidence intervals. In this sense, the models broadly agree, with the individual 1σ intervals usually overlapping the combined 1σ region or fractionally separated but we note a few exceptions. First, the mixing-length parameter for the free power-law correction tends to be larger than for the other corrections. In addition, the results for stars C and E appear to be the least consistent. We have already noted the flaws in our models of star E but it is not clear what disrupts the fits in star C.

We also compared the standard deviations of the central best-fit values with the individual uncertainties. There is great variation in this ratio but we can roughly say that the uncertainty in each parameter introduced by the choice of surface effect is between one and two times the uncertainty in each individual fit. Put differently, one can say that the choice of surface correction biases the results relative to one another but usually by no more than the 2σ uncertainties. The cubic and combined terms by Ball & Gizon (2014) obviously agree better – almost always within the mutual 1σ limits – because the cubic correction is a special case of the combined correction.

As a third comparison of the uncertainties, we combined the results for each star for each variable in Tables 3 and 4, assuming that the results are from uncorrelated normal distributions. The overall uncertainties, which now span the full ranges covered by the fours surface corrections, are usually between 2 and 3 times the uncertainties for the individual fits. Relative to the best-fitting values, for the masses M, radii R and ages t, we find that the total uncertainties are always less than about 2, 1 and 6 per cent, respectively.

3.5. Mixing-length parameters

Since the landmark work by Ludwig et al. (1999), two- and three-dimensional radiation hydrodynamics simulations of near-surface convection have allowed for calibration of the mixing-length parameter α for cool stars of various types. In recent years, several suites of simulations have been used to perform such calibration (e.g. Trampedach et al. 2014; Magic et al. 2015) and consistently conclude that, roughly speaking, the mixing-length parameter should decrease as the effective temperature increases or the surface gravity decreases.

The tables produced by Magic et al. (2015) include calibrations for different metallicities [Fe/H] and allow us to compare our mixing-length parameters with those predicted from their calibration. For each star, we generated 10^5 realizations of $\Delta\nu$, $\nu_{\max}$, $T_{\rm eff}$ and [Fe/H] and used them to interpolate in the data of Magic et al. (2015), using the mixing-length parameters calibrated to the entropy at the bottom boundary of the simulation. (Using the calibration to the entropy jump gives nearly identical results.) Table 5 shows the means and standard deviations of the samples for each star, divided by the solar value, which itself depends on the choice of atmospheric model and detailed implementation of mixing-length theory. This table also gives the ratio multiplied by our solar-calibrated value $\alpha_{\odot,\rm MESA} = 1.788$. The simulation calibrations consistently suggest that the mixing-length parameter $\alpha_{\rm MLT}$ should be less than the solar-calibrated value. In our fits, we have found the opposite: $\alpha_{\rm MLT}$ is larger than the solar value, mostly falling between 1.8 and 2.1.

Table 5. Mixing-length parameters predicted by linear interpolation in the grid of values calibrated to Stagger simulations by Magic et al. (2015).

Star	$\alpha/\alpha_{\odot,\rm STAGGER}$	$\times\alpha_{\odot,\rm MESA}$
A	0.982 ± 0.033	1.755 ± 0.059
B	0.961 ± 0.005	1.718 ± 0.008
C	0.944 ± 0.105	1.688 ± 0.188
D	0.978 ± 0.014	1.749 ± 0.025
E	0.933 ± 0.061	1.668 ± 0.109
F	0.880 ± 0.064	1.574 ± 0.115

Notes. The second column gives the mixing-length parameter relative to the value of their solar simulation. The third column gives this ratio multiplied by the solar-calibrated mixing-length parameter for our stellar models, $\alpha_{\odot,\rm MESA}$.

What causes this discrepancy? Based on their ability to reproduce observable features of solar granulation, the simulations are generally regarded as reasonably realistic, at least for the Sun (see e.g. Nordlund et al. 2009, for a review). In addition, there is already some observational support for small mixing-length parameters on the red giant branch. Piau et al. (2011) modelled a range of stars across the red giant branch ($3.8 > \log g > 1.5$) for which linear diameters could be determined to better than 10 per cent, and found that they were much better able to model the stars with a sub-solar value for the mixing-length parameter.

Given the strong correlations between the parameters, our mixing-length parameters are probably being used to adjust the stellar radii so that the mode frequencies match the observations. The incorrect part of the stellar model could then instead be, for example, the initial helium abundance Y_0, the gravitational settling or another component of the input physics. It remains to be seen if this effect persists in asteroseismic models of subgiants and low-luminosity red giants or if it is specific to the fits presented here.

4. Conclusion

We have modelled the individual mode frequencies of six subgiants and low-luminosity red giants using five different parametrizations of the surface effects. The solar-calibrated power-law correction proposed by Kjeldsen et al. (2008) is clearly unsuitable, consistently producing much poorer fits and often converging on models without any surface effect. This poor performance is not surprising: there is no reason to expect a solar-calibrated correction to work on evolved stars that are unlike the present Sun.

The remaining four surface corrections provide fits of similar quality, with the combined correction by Ball & Gizon (2014) being marginally superior for most of the stars. The best-fitting parameters of these four sets of fits are generally mutually agreeable within the 2σ uncertainties, with the exception that the parameters found with the modified Lorentzian or free power law

occasionally disagree at slightly more than the mutual 3σ level. Put differently, the systematic uncertainty is roughly twice the statistical uncertainty in our fits (though it varies for different parameters). For the masses, radii and ages of the stars, the total fractional uncertainties are always smaller than about 2, 1 and 6 per cent, respectively.

Finally, we note that the present results demonstrate that the individual mode frequencies of these subgiants and low-luminosity red giants can be used to constrain models, in much the same fashion as is now commonplace for main-sequence dwarfs. Our modelling procedure is only marginally different from what has already been used for dwarf solar-like oscillators, almost entirely in allowing shorter timesteps to resolve the rapid evolution of the mixed mode frequencies. Even given the additional uncertainty introduced by the surface correction, the model parameters of these stars can help to precisely constrain the physics of stellar interiors.

Acknowledgements. The authors acknowledge research funding by Deutsche Forschungsgemeinschaft (DFG) under grant SFB 963/1 "Astrophysical flow instabilities and turbulence", Project A18. L.G. acknowledges support by the Center for Space Science at the NYU Abu Dhabi Institute under grant G1502.

References

Angulo, C., Arnould, M., Rayet, M., et al. 1999, Nucl. Phys. A, 656, 3
Appourchaux, T., Antia, H. M., Ball, W. H., et al. 2015, A&A, 582, A25
Auvergne, M., Bodin, P., Boisnard, L., et al. 2009, A&A, 506, 411
Ball, W. H., & Gizon, L. 2014, A&A, 568, A123
Ball, W. H., Beeck, B., Cameron, R. H., & Gizon, L. 2016, A&A, 592, A159
Böhm-Vitense, E. 1958, ZAp, 46, 108
Borucki, W. J., Koch, D., Basri, G., et al. 2010, Science, 327, 977
Caughlan, G. R., & Fowler, W. A. 1988, Atomic Data and Nuclear Data Tables, 40, 283
Charbonneau, P., & Michaud, G. 1991, ApJ, 370, 693
Christensen-Dalsgaard, J. 1986, in Seismology of the Sun and the distant stars: Proc. NATO Adv. Res. Workshop, Cambridge, England, June 17–21, 1985, ed. D. O. Gough (Dordrecht: D. Reidel Publishing Co.), NATO Adv. Sci. Inst. (ASI) Series C, 169, 23
Christensen-Dalsgaard, J. 2008, Ap&SS, 316, 113
Christensen-Dalsgaard, J., & Berthomieu, G. 1991, in Solar Interior and Atmosphere, eds. A. N. Cox, W. C. Livingston, & M. S. Matthews (Tuscon: University of Arizona Press), 401
Cox, J. P., & Giuli, R. T. 1968, Principles of stellar structure (New York: Gordon and Breach)
Cyburt, R. H., Fields, B. D., Olive, K. A., & Yeh, T.-H. 2016, Rev. Mod. Phys., 88, 015004
Deheuvels, S., Doğan, G., Goupil, M. J., et al. 2014, A&A, 564, A27
Ferguson, J. W., Alexander, D. R., Allard, F., et al. 2005, ApJ, 623, 585
Gough, D. O. 1990, in Progress of Seismology of the Sun and Stars, eds. Y. Osaki, & H. Shibahashi (Berlin: Springer Verlag), Lecture Notes in Physics, 367, 283
Grevesse, N., & Sauval, A. J. 1998, Space Sci. Rev., 85, 161
Hekker, S., & Christensen-Dalsgaard, J. 2016, A&ARv, submitted [arXiv:1609.07487]
Houdek, G., Trampedach, R., Aarslev, M. J., & Christensen-Dalsgaard, J. 2017, MNRAS, 464, L124
Iglesias, C. A., & Rogers, F. J. 1996, ApJ, 464, 943
Imbriani, G., Costantini, H., Formicola, A., et al. 2005, Eur. Phys. J. A, 25, 455
Jiménez, A., García, R. A., & Pallé, P. L. 2011, ApJ, 743, 99
Kjeldsen, H., & Bedding, T. R. 1995, A&A, 293, 87
Kjeldsen, H., Bedding, T. R., & Christensen-Dalsgaard, J. 2008, ApJ, 683, L175
Kunz, R., Fey, M., Jaeger, M., et al. 2002, ApJ, 567, 643
Ludwig, H.-G., Freytag, B., & Steffen, M. 1999, A&A, 346, 111
Lund, M. N., Silva Aguirre, V., Davies, G. R., et al. 2017, ApJ, 835, 172
Magic, Z., & Weiss, A. 2016, A&A, 592, A24
Magic, Z., Weiss, A., & Asplund, M. 2015, A&A, 573, A89
Metcalfe, T. S., Chaplin, W. J., Appourchaux, T., et al. 2012, ApJ, 748, L10
Metcalfe, T. S., Creevey, O. L., Doğan, G., et al. 2014, ApJS, 214, 27
Michaud, G., Richer, J., & Vick, M. 2011, A&A, 534, A18
Nelder, J. A., & Mead, R. 1965, The Comput. J., 7, 308
Nordlund, Å., Stein, R. F., & Asplund, M. 2009, Liv. Rev. Sol. Phys., 6
Otí Floranes, H., Christensen-Dalsgaard, J., & Thompson, M. J. 2005, MNRAS, 356, 671
Paxton, B., Bildsten, L., Dotter, A., et al. 2011, ApJS, 192, 3
Paxton, B., Cantiello, M., Arras, P., et al. 2013, ApJS, 208, 4
Paxton, B., Marchant, P., Schwab, J., et al. 2015, ApJS, 220, 15
Pérez Hernández, F., García, R. A., Corsaro, E., Triana, S. A., & De Ridder, J. 2016, A&A, 591, A99
Piau, L., Kervella, P., Dib, S., & Hauschildt, P. 2011, A&A, 526, A100
Piau, L., Collet, R., Stein, R. F., et al. 2014, MNRAS, 437, 164
Reese, D. R., Chaplin, W. J., Davies, G. R., et al. 2016, A&A, 592, A14
Rogers, F. J., & Nayfonov, A. 2002, ApJ, 576, 1064
Rosenthal, C. S., Christensen-Dalsgaard, J., Nordlund, Å., Stein, R. F., & Trampedach, R. 1999, A&A, 351, 689
Roxburgh, I. W. 2015, A&A, 574, A45
Roxburgh, I. W. 2016, A&A, 585, A63
Roxburgh, I. W., & Vorontsov, S. V. 2003, A&A, 411, 215
Schmitt, J. R., & Basu, S. 2015, ApJ, 808, 123
Silva Aguirre, V., Lund, M., Antia, H. M., et al. 2017, ApJ, 835, 173
Sonoi, T., Samadi, R., Belkacem, K., et al. 2015, A&A, 583, A112
Thoul, A. A., Bahcall, J. N., & Loeb, A. 1994, ApJ, 421, 828
Trampedach, R., Stein, R. F., Christensen-Dalsgaard, J., Nordlund, Å., & Asplund, M. 2014, MNRAS, 445, 4366
Turcotte, S., Richer, J., & Michaud, G. 1998, ApJ, 504, 559